Identification of a dipole band above the $I^\pi = 31/2^-$ isomeric state in ^{189}Pb

D. Hodge,[1] D. M. Cullen,[1] M. J. Taylor,[1] M. G. Procter,[1] P. Nieminen,[2] T. Grahn,[2] P. T. Greenlees,[2] K. Hauschild,[2,*] A. Herzan,[2] U. Jakobsson,[2,†] P. Jones,[3] R. Julin,[2] S. Juutinen,[2] S. Ketelhut,[2] M. Leino,[2] A. Lopez-Martens,[2,*] J. Partanen,[2] P. Peura,[2] P. Rahkila,[2] S. Rinta-Antila,[2] P. Ruotsalainen,[2,‡] M. Sandzelius,[2] J. Sarén,[2] C. Scholey,[2] J. Sorri,[2] S. Stolze,[2] and J. Uusitalo[2]

[1]*School of Physics & Astronomy, Schuster Laboratory, The University of Manchester, Manchester M13 9PL, United Kingdom*

[2]*University of Jyvaskyla, Department of Physics, P.O. Box 35, FIN-40014 Jyvaskyla, Finland*

[3]*Department of Nuclear Physics, iThemba LABS, P.O. Box 722, Somerset West 7129, South Africa*

(Received 1 May 2015; revised manuscript received 12 October 2015; published 17 November 2015)

A dipole band of six transitions built upon a firmly established $I^\pi = 31/2^-$ isomeric state has been identified in ^{189}Pb using recoil-isomer tagging. This is the lightest odd-mass Pb nucleus in which a dipole band is known. The dipole nature of the new transitions has been confirmed through angular-intensity arguments. The evolution of the excitation energy and the aligned-angular momentum of the states in the new dipole band are compared with those of dipole bands in heavier, odd-mass lead isotopes. This comparison suggests that the new band in ^{189}Pb is based upon a $\pi[s_{1/2}^{-2}h_{9/2}i_{13/2}]_{11^-} \otimes \nu[i_{13/2^+}^{-1}]_{13/2^+}$ configuration. However, the increased aligned-angular momentum in ^{189}Pb may suggest evidence for a reduced repulsive proton/neutron-hole interaction compared to dipole bands in the heavier mass isotopes.

DOI: 10.1103/PhysRevC.92.054312 PACS number(s): 23.20.Lv, 21.10.Re, 23.20.En, 27.70.+q

I. INTRODUCTION

The neutron-deficient, odd-mass, Pb isotopes are known to exhibit a wide variety of nuclear shapes and structures [1]. These range from single-particle configurations associated with the coupling of a single-unpaired neutron to the even-mass nuclear core at low excitation energies [2–6], through triple-shape coexisting states at intermediate excitation energies [7,8], to highly collective superdeformed structures at the highest excitation energies [9]. The particular behavior depends on the competition between collective effects from the many neutrons in the middle of the $N = 82$–126 shell and noncollective effects associated with the protons at the fully paired $Z = 82$ shell closure [10].

A common feature of this region is the existence of dipole bands with strong $M1$ and weak $E2$ transitions in weakly deformed nuclei [2–6,8,11–13]. These dipole bands originate from the coupling of protons in the $h_{9/2}$ orbital to neutron holes in the $i_{13/2}$ orbital [10,12,13]. At the band head, the projections of the neutron and proton states are near perpendicular to each other due to the repulsive particle-hole interaction. The total angular momentum, $\bar{I}$, therefore points somewhere between the proton and neutron angular momenta. Higher angular momentum states in the band are formed by the stepwise alignment of the neutron and proton angular momenta with $\bar{I}$. This mechanism is known as the shears mode, due to the alignment of the proton and neutron orbits resembling the closing of a pair of shears [12,13]. For the odd-mass, Pb nuclei, with $A = 191$–199, the most intense shears-mode dipole bands are based upon a $\pi[s_{1/2}^{-2}h_{9/2}i_{13/2}]_{11^-} \otimes \nu[i_{13/2}^{-1}]_{13/2^+}$ configuration [2–6]. The next lightest isotope in this chain, ^{189}Pb, might also be expected to form a dipole band built upon these orbits.

An isomeric state with a mean lifetime of $\tau = 32^{+10}_{-2}\mu$s was discovered in ^{189}Pb by Baxter *et al.* [14], but was not definitively linked to the lower-spin states. However, subsequent work by Dracoulis *et al.* firmly assigned the spin and parity of the isomer to be $I^\pi = 31/2^-$ using detailed γ-ray and internal conversion electron spectroscopic measurements [10]. Dracoulis *et al.* also first proposed that the $I^\pi = 31/2^-$ state was likely to be a shears-mode band head. As reported in Ref. [10], this band-head spin was predicted to be higher than those of the most intense shears-mode bands in the heavier Pb nuclei [2–6]. This increase in spin was thought to be due to the decreased residual interaction between the two proton $\pi s_{1/2}^{-2}h_{9/2}i_{13/2}$ excitation and the $i_{13/2}$ neutron-hole excitation. The residual interaction between these excitations is repulsive and so favors a perpendicular coupling of the angular momentum projections. As the $i_{13/2}$ neutron shell is depleted in the lighter Pb nuclei, the neutron quasiparticle excitation becomes less hole-like resulting in a weaker repulsive interaction and a corresponding increase in the alignment of the two configurations. This is reflected by an increase in band-head spin towards the midshell.

In the present paper, the first evidence is presented for six newly identified transitions, which form a dipole band built upon the $I^\pi = 31/2^-$ isomeric state in ^{189}Pb. This measurement extends the established "island" of dipole bands into the lighter-mass Pb isotopes. It may represent one of the lightest Pb isotopes in which dipole bands built on configurations including the $i_{13/2}$ neutron orbital are observed. This is due to the falling neutron Fermi level, which results in a higher relative excitation energy, and by corollary, a reduced occupation of the $i_{13/2}$ orbital. The excitation energy and

*Present address: CSNSM-IN2P3-CNRS, Université Paris-Sud, 91406 Orsay, France.

†Present address: KTH The Division of Nuclear Physics, AlbaNova University Center, SE-106 91 Stockholm, Sweden.

‡Present address: TRIUMF, 4004 Wesbrook Mall, Vancouver, BC V6T 2A3, Canada.

aligned-angular momentum of the new ^{189}Pb states established in this work are compared with those of existing dipole bands in the neighboring heavier-mass isotopes; ^{191}Pb to ^{199}Pb. This comparison also suggests that the new band in ^{189}Pb is based upon a $\pi[s_{1/2}^{-2}h_{9/2}i_{13/2}]_{11^-} \otimes \nu[i_{13/2}^{-1}]_{13/2^+}$ configuration.

II. EXPERIMENTAL DETAILS

The fusion-evaporation reaction ^{106}Pd(^{86}Kr,$3n$) was used to populate excited states in ^{189}Pb. A beam of ^{86}Kr was accelerated to an energy of 355 MeV using the K130 cyclotron at the Accelerator Laboratory of the University of Jyväskylä. The beam, with an average current of 10 pnA, was directed onto a 500 μg/cm^2 ^{106}Pd target for a total of ∼150 hrs. The JUROGAM-II array surrounded the target position to detect prompt γ-ray decays. JUROGAM-II consisted of 39 Compton-suppressed high-purity germanium detectors with a photo-peak efficiency of ∼6% at 1.3 MeV. The JUROGAM-II detectors were arranged into four separate rings with different angles to the beam axis: Ring 1 (157.6°, 5 phase 1 detectors), Ring 2 (133.6°, 10 phase 1 detectors), Ring 3 (104.5°, 12 clover detectors) and Ring 4 (75.5°, 12 clover detectors) [15]. The average rates for the phase 1 and clover detectors during the experiment were ∼18 kHz and ∼36 kHz respectively. From the target position, the recoiling nuclei were transported, with a velocity of $v/c = 4.0\%$, through the gas-filled recoil ion transportation unit (RITU) [16], in order to separate scattered beam from the recoiling reaction products. Upon leaving RITU, the recoils pass through a multiwire proportional counter (MWPC) before implanting in one of two double-sided silicon strip detectors (DSSDs). The average DSSD rate throughout the experiment was ∼6.4 kHz. The MWPC and DSSDs form the GREAT focal-plane spectrometer along with three clover germanium detectors and a planar germanium detector [17]. The GREAT germanium detectors allowed the detection of isomeric γ-ray decays, as well as those emitted after the β-decay of implanted nuclei. The planar detector was placed directly behind the DSSDs to detect low energy γ rays, while the three clover detectors were placed perpendicular to the sides and top of the DSSDs to detect higher-energy γ rays. All detector events were time stamped by the total data readout (TDR) system [18], which allowed the correlation of different detector events. Events were sorted online using the GRAIN software package [19] and analyzed using the RADWARE suite of programs [20]. In this work, all events analyzed were recoil tagged by imposing gates on the energy loss of recoils in the MWPC and the time of flight between the MWPC and DSSDs in order to separate recoils from any scattered or primary beam in the DSSDs. In addition, recoil-isomer tagging was used to correlate prompt JUROGAM-II γ rays (γ_p) with the delayed γ rays (γ_d) in the GREAT clover and planar detectors for recoil-gated events [21].

III. RESULTS

In order to determine the relative yields of the various reaction channels populated in the experiment, a recoil-tagged prompt γ_p-γ_p matrix was initially constructed. For prompt γ rays to be included in this matrix they had to be detected within 150 ns of each other. In this matrix, the yrast transitions from ^{189}Pb were observed to constitute ∼28% of the observed γ-ray intensity. The other main channels observed were ^{188}Pb ($4n$, ∼28%), ^{189}Tl ($1p2n \sim 26\%$), and ^{186}Hg ($2n\alpha \sim 9\%$). In order to correlate prompt (JUROGAM-II) and delayed (GREAT clovers and planar) events across isomeric states, recoil-isomer tagged matrices were created. Delayed γ rays were only included in these matrices if they were detected between 0−60 μs after a recoil implantation in the DSSDs. This time gate corresponds to approximately three half-lives of the known $I^\pi = 31/2^-$, $\tau = 32^{+10}_{-2}$ μs isomeric state in ^{189}Pb [10]. A background of random correlation events, and β-delayed γ-ray decays from previously implanted recoils, were subtracted from these matrices if they were detected up to 43 μs before the recoil implant in the DSSD. These limits were found to give the best peak-to-background ratio in the recoil-isomer tagged spectra and were subsequently imposed on all recoil-isomer tagged matrices in this work. Figure 1 shows delayed total projection spectra from two γ_p-γ_d matrices: Fig. 1(a), a JUROGAM-II versus GREAT clover detectors matrix and Fig. 1(b), a JUROGAM-II versus GREAT planar detector matrix. Although the main delayed transitions in these projections are from ^{189}Pb [10], delayed contaminant transitions from a known $\tau = 1.2$ μs isomer in ^{188}Pb [11] and known $\tau = 11$ μs and $\tau = 36$ μs isomers in ^{190}Pb [8] were also found to strongly correlate with the 0−60 μs recoil-isomer time gate used in the matrices.

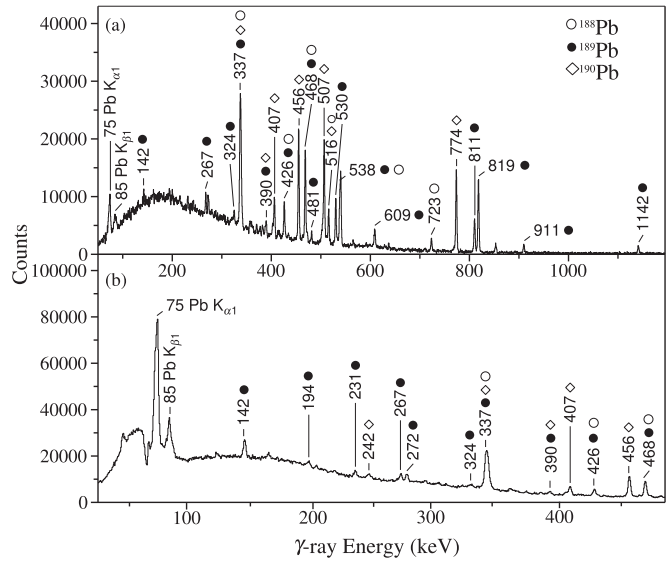

FIG. 1. Delayed total projections from the prompt-delayed (γ_p-γ_d) matrices for (a) the GREAT clover detectors and (b) the GREAT planar detector. The timing conditions imposed on the matrix are discussed in the text.

In order to avoid any potential contamination when gating on the transitions below the $I^\pi = 31/2^-$ isomeric state in ^{189}Pb, a recoil-isomer tagged γ_d-γ_d, GREAT planar versus clovers matrix was created with the same time gates as discussed previously. For delayed γ rays to be included in this matrix they had to be detected within 150 ns of each other. The matrix was used to identify nine uncontaminated

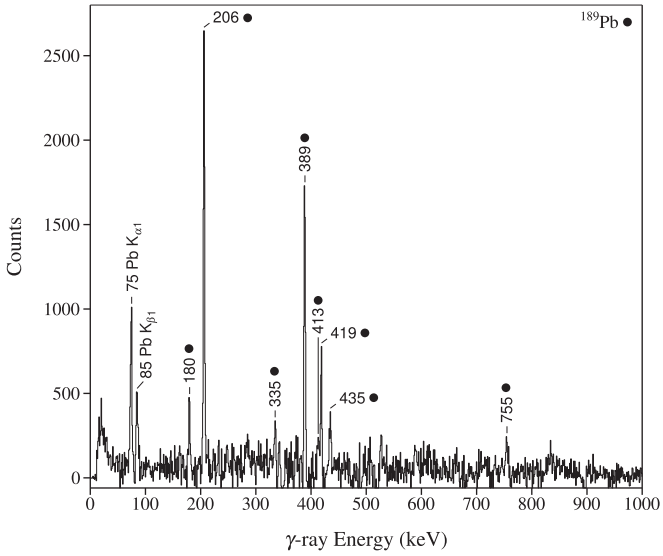

FIG. 2. Newly established prompt transitions above the $I^{\pi} = 31/2^{-}$ isomeric state in ^{189}Pb from a sum of delayed gates in an isomer-tagged γ_p-γ_d matrix, see text for details.

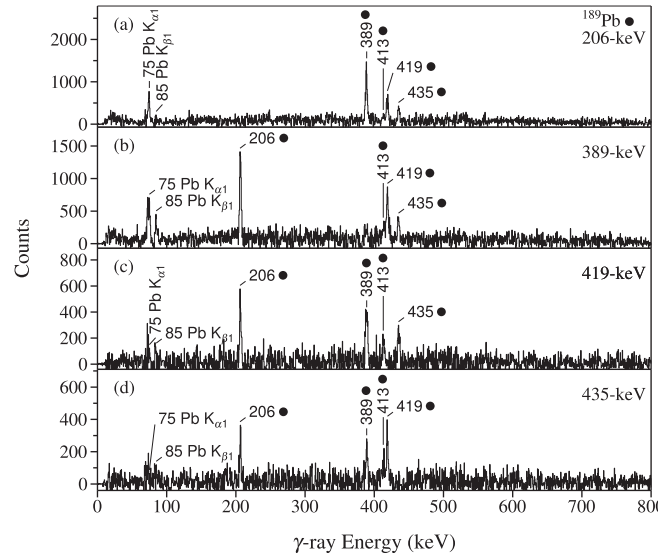

FIG. 3. Recoil-isomer tagged prompt γ_p-γ_p coincidence spectra gated by (a) 206-, (b) 389-, (c) 419-, and (d) 435-keV transitions above the $I^{\pi} = 31/2^{-}$ isomeric state in ^{189}Pb [10]. The timing conditions are as described in the text.

transitions below the known $I^{\pi} = 31/2^{-}$ isomeric state in ^{189}Pb [10]. These were found to be the 142-, 267-, and 272-keV transitions from gates set in the planar detector and the 530-, 609-, 811-, 819-, 911-, and 1142-keV transitions from gates set in the clover detectors. These uncontaminated delayed transitions were then used as gates in the recoil-isomer tagged prompt-delayed (γ_p-γ_d) matrices to produce a sum spectrum of prompt ^{189}Pb transitions. Figure 2 shows this spectrum of eight correlated prompt γ-ray decays with energies of 180-, 206-, 335-, 389-, 413-, 419-, 435-, and 755-keV. These transitions are not known in the literature [10,14,22,23] and are proposed to lie above the $I^{\pi} = 31/2^{-}$ isomeric state in ^{189}Pb [10].

In order to check whether any of these new prompt transitions were coincident with each other, a recoil-isomer tagged prompt γ_p-γ_p matrix was created using the JUROGAM-II detectors with the timing and coincidence conditions discussed previously. Figure 3 shows spectra gated by the new 3(a) 206-, 3(b) 389-, 3(c) 419-, and 3(d) 435-keV transitions in the recoil-isomer tagged prompt γ_p-γ_p matrix. From these gates, it was concluded that the 206-, 389-, 419-, 435-, and 413-keV γ rays are all in prompt coincidence with each other above the $I^{\pi} = 31/2^{-}$ isomeric state in ^{189}Pb [10]. The ordering of the new prompt transitions was established using the γ-ray intensities, corrected for efficiency and internal conversion [24], from the recoil-isomer tagged spectrum shown in Fig. 2. The relative γ-ray intensities from the spectrum are listed in Table I(a).

In addition to this main sequence of γ-ray transitions above the $I^{\pi} = 31/2^{-}$ isomeric state, Fig. 2 reveals the presence of three other transitions with energies of 180-, 335-, and 755-keV. These transitions do not show any firm γ_p-γ_p coincidences with the main sequence of γ rays shown in Fig. 3. However, when prompt gates are set on the 180-, 335-, and 755-keV energy transitions in the prompt-delayed (γ_p-γ_d) matrices, the correlated delayed spectra only show known delayed decays from the $I^{\pi} = 31/2^{-}$ isomeric state in ^{189}Pb [10], see Fig. 4. This reveals that these transitions are from excited states above the $I^{\pi} = 31/2^{-}$ isomeric state. The lack of any prompt γ_p-γ_p coincidences with transitions in the main band, have led to the 755- and 180-keV transitions being tentatively placed directly above the isomeric state.

TABLE I. (a) Relative efficiency-corrected γ-ray intensities and angular intensity ratios of the newly observed, prompt γ rays above the $I^{\pi} = 31/2^{-}$ state in ^{189}Pb and (b) the angular intensity ratios of known stretched $M1$ and $E2$ transitions in ^{189}Tl.

Prompt γ-ray energy (keV)	I_{γ}	$I^{\pi}_{\text{initial}} \rightarrow I^{\pi}_{\text{final}}$	Ring 1 Intensity versus Ring 4 Intensity
(a) ^{189}Pb			
179.8(3)	166(4)	$(33/2^{+}) \rightarrow 31/2^{-}$	0.49(6)
206.4(1)	999(16)	$33/2^{-} \rightarrow 31/2^{-}$	0.56(5)
335.1(6)	183(9)	$(43/2^{-}) \rightarrow (41/2^{-})$	0.38(13)
388.8(2)	1000(17)	$35/2^{(-)} \rightarrow 33/2^{-}$	0.49(6)
413.2(3)	167(7)	$(41/2^{-}) \rightarrow (39/2^{-})$	0.69(24)
418.7(3)	396(10)	$37/2^{(-)} \rightarrow 35/2^{(-)}$	0.44(10)
435.0(3)	247(8)	$(39/2^{-}) \rightarrow 37/2^{(-)}$	0.62(17)
754.5(10)	198(9)	$(33/2^{-}) \rightarrow 31/2^{-}$	0.36(20)
(b) ^{189}Tl			
314.4(1)		$13/2^{-} \rightarrow 11/2^{-}$	0.51(6)
139.1(2)		$25/2^{-} \rightarrow 23/2^{-}$	0.56(6)
			$M1$ weighted average = 0.54(4)
700.2(1)		$13/2^{-} \rightarrow 9/2^{-}$	1.04(5)
502.5(2)		$23/2^{-} \rightarrow 19/2^{-}$	1.08(3)
			$E2$ weighted average = 1.07(3)

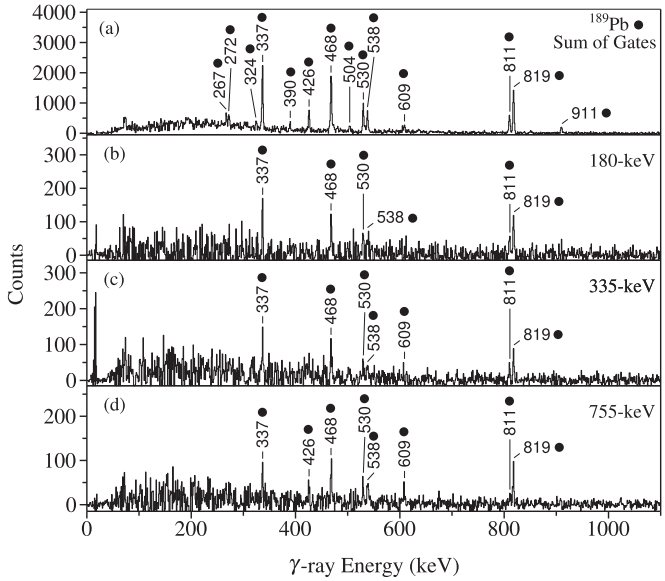

FIG. 4. Recoil-isomer tagged delayed γ_p-γ_d coincidence spectra gated by (a) 206-, 389-, 419-, 413-, and 435-keV (b) 180-, (c) 335-, and (d) 755-keV transitions above the $I^\pi = 31/2^-$ isomeric state in ^{189}Pb [10]. The timing conditions imposed on the matrix are described in the text.

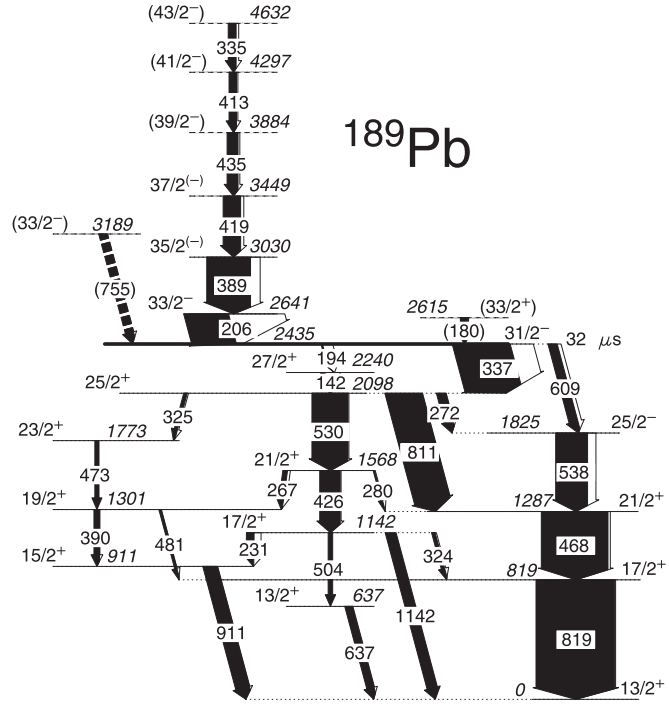

FIG. 5. Partial level scheme showing the prompt ^{189}Pb transitions above the $I^\pi = 31/2^-$ isomeric state from this work and the previously known delayed transitions from Ref. [10]. Excitation energies are quoted relative to the long-lived $I^\pi = 13/2^+$ isomer.

From the statistics available in the recoil-isomer tagged γ_p-γ_p matrix it is inconclusive whether the 335-keV transition is in coincidence with the other newly identified transitions due to its low intensity. However, systematic arguments, presented in Sec. IV, have led to its placement above the 413-keV transition in the newly identified sequence. The new partial level scheme, for the prompt ^{189}Pb transitions above the $I^\pi = 31/2^-$ isomer, is shown in Fig. 5.

Angular-intensity ratios were used to determine whether the newly established prompt ^{189}Pb γ rays were predominantly of dipole or quadrupole nature. Rings 1 and 4 of JUROGAM-II were used for the analysis as they provided the maximum angular separation required (157.6°–75.5°). From a recoil-tagged matrix, dipole and quadrupole control ratios were first calculated for large intensity transitions with known multipolarities in the neighboring nucleus ^{189}Tl [25], see Table I(b). For the ^{189}Pb transitions, the intensities were taken from recoil-isomer tagged Ring 1 versus focal-plane clover and Ring 4 versus focal-plane clover matrices. The timing conditions applied to these matrices were the same as discussed earlier in the text.

The angular-intensity ratios assign the majority of the new prompt ^{189}Pb transitions above the $I^\pi = 31/2^-$ isomer as dipoles. The 180-, 206-, 335-, 389-, 419-, and 755-keV transitions are unambiguously defined. The measured ratios for these transitions do not overlap within 3σ with the quadrupole ratio from the strong neighboring transitions. However, the 413- and 435-keV transitions are not unambiguously defined.

Conversion coefficient analysis was attempted to further characterise the newly assigned dipole transitions as either $M1$ or $E1$ transitions. The extraction of internal conversion coefficients from total intensity flow analysis was only possible for the 206-keV transition that directly feeds the $I^\pi = 31/2^-$ isomeric state. The 206-keV internal conversion coefficient was calculated from the ratio of γ- and x-ray intensities from the recoil-isomer tagged $\gamma_p - \gamma_p$ matrix with a gate set on the 389-keV transition, see Fig. 3(b) and Table II. In the calculation, the theoretical x-ray intensity from the internal conversion of the additional 419-, 435-, and 413-keV γ-rays in Fig. 3(b) was first subtracted from the total x-ray intensity using the values in Table II. In the calculation it was assumed that all of these transitions were of stretched $M1$ character and the associated internal conversion coefficients were taken from the BrIcc database [24]. The ratio of the remaining K x-ray intensity and the 206-keV γ-ray intensity was then used to calculate an internal conversion coefficient of $\alpha_k = 1.11(4)$

TABLE II. The efficiency-corrected Pb K x-ray and prompt γ-ray intensities from the 389-keV gated spectrum shown in Fig. 3(b) and associated BrIcc theoretical internal conversion coefficients, α_k, for the cases of the transitions having stretched $E1$ or $M1$ multipolarities [24].

$E_{\text{x-ray}}$ or E_γ (keV)	I_γ	BrIcc	
		$\alpha_k(M1)$	$\alpha_k(E1)$
$K_{\alpha1}$ 75.0	4356(81)		
$K_{\beta1}$ 84.9	1277(50)		
206.4(1)	4120(100)	0.9840(140)	0.0590(9)
413.2(3)	1367(56)	0.1471(21)	0.0119(2)
418.7(3)	4564(83)	0.1415(20)	0.0115(2)
435.0(3)	1804(72)	0.1280(18)	0.0106(2)

for the 206-keV transition. The calculated 206-keV α_k value is consistent within 3σ with the BrIcc database [24] value $\alpha_k(M1) = 0.984(14)$, but not with $\alpha_k(E1) = 0.0590(9)$. The conversion coefficient analysis, hence, shows that the new 206-keV transition has an $M1$ rather than an $E1$ multipolarity. If the calculation is repeated assuming the 419-, 435-, and 413-keV γ rays are stretched $E1$ transitions, then the resulting conversion coefficient for the 206 keV transition is 1.35(4). The fact that this does not overlap with either of the BrIcc values adds weight to the suggestion that the higher lying transitions are of $M1$ nature.

IV. DISCUSSION

In this work, the observation of transitions built upon the $I^\pi = 31/2^-$ isomeric state in ^{189}Pb aids its assignment as a shears-mode band-head state. Through angular distribution ratios, the majority of the newly observed ^{189}Pb transitions were designated as dipoles, see Table I. Additionally, the 206-keV transition was confirmed as a magnetic dipole from its calculated internal conversion coefficient. Although this does not rule out the possibility that the rest of the newly observed transitions have an $E1$ multipolarity, such a sequence would be quite unusual. Since dipole bands based on sequences of $M1$ transitions are common in the neutron-deficient Pb isotopes, it is suggested that these five coincident dipole transitions at energies 206-, 389-, 419-, 435-, and 413-keV also form an $M1$ dipole band above the $I^\pi = 31/2^-$ isomeric state. The prompt transitions, with energies of 180- and 755-keV, are tentatively placed as directly feeding the $I^\pi = 31/2^-$ isomeric state. In this scenario, the greater intensity of the 206-keV transition indicates that the $I^\pi = 33/2^-$ state it depopulates must be the yrast $I^\pi = 33/2^-$ state and that the lower-lying state depopulated by the 180-keV transition has a different spin or parity. As the 180-keV transition is a firmly assigned dipole, see Table I, it is tentatively designated as an $E1$ transition. The 755-keV transition is assigned as a dipole from its angular distribution ratios but is not firmly assigned as either an $E1$ or $M1$ transition. Despite the lack of firm prompt γ-ray coincidences, the 335-keV transition is placed above the 413-keV transition in the dipole band. This placement is consistent with the existing systematics of rotational frequency and aligned-angular momenta (see below) seen in the most intense dipole band states in heavier odd-mass Pb nuclei.

Figure 6(a) shows the aligned-angular momentum, i_x, as a function of rotational frequency for the most intense dipole bands in the odd-mass ^{191}Pb - ^{199}Pb isotopes [2,4–6,26]. The figure also shows the data for the new dipole band in ^{189}Pb (filled circles) including the 335-keV $(43/2^-)$ to $(41/2^-)$ transition tentatively placed on the top of the dipole band. Each band has been plotted assuming $K = 11$ and has a reference band with Harris parameters $\Im_0 = 10.0\hbar^2/\text{MeV}$ and $\Im_1 = 30.0\hbar^4/\text{MeV}^3$ subtracted in accordance with Ref. [2].

The negative parity dipole bands in the nuclei ^{191}Pb - ^{199}Pb are known to be built upon the $\pi[s_{1/2}^{-2}h_{9/2}i_{13/2}]_{11^-} \otimes \nu[i_{13/2}^{-1}]_{13/2^+}$ configuration at low rotational frequencies and the $\pi[s_{1/2}^{-2}h_{9/2}i_{13/2}]_{11^-} \otimes \nu[i_{13/2}^{-3}]_{33/2^+}$ configuration at higher rotational frequencies above the first band crossing [2,4–6,26].

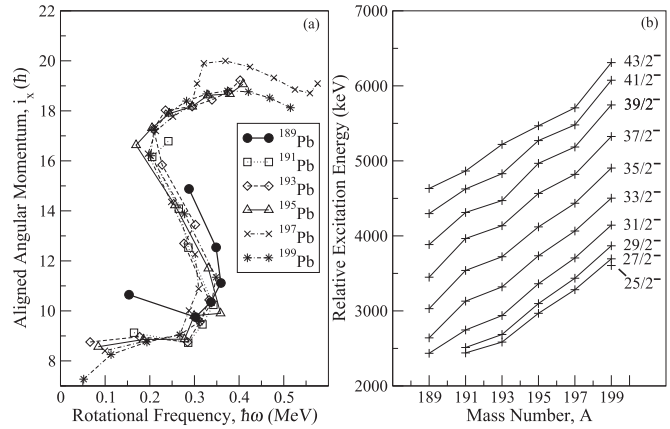

FIG. 6. The systematics of the strongest dipole bands in ^{191}Pb - ^{199}Pb [2,4–6,26] with the new data for ^{189}Pb (filled circles). Shown are: (a) the aligned-angular momentum as a function of rotational frequency and (b) the excitation energy of states with spins between $25/2^-$ and $43/2^-$, relative to the $13/2^+$ neutron-hole excitation.

This first band crossing involves the alignment of two $i_{13/2}$ neutrons and takes place around rotational frequencies of $\hbar\omega \approx 0.30$–0.36 MeV, with an aligned-angular momentum gain of 8–9$\hbar$ [2–6]. From Fig. 6(a), it can be seen that the new dipole band built upon the $I^\pi = 31/2^-$ isomeric state in ^{189}Pb (filled circles) follows the general alignment trend of known dipole bands in these odd-mass Pb isotopes [2–6]. The crossing frequency of $\hbar\omega \approx 0.36$ MeV for the ^{189}Pb dipole band is within the range of frequencies seen in dipole bands of the heavier Pb isotopes. Although the full extent of the aligned-angular momentum gain due to the band crossing is not established in ^{189}Pb, the gain of $\Delta i_x > 6\hbar$ agrees with that seen in the heavier isotopes within the extent of the present data. Based on these comparisons, the new dipole band in ^{189}Pb is expected to be built upon a similar structure involving the $\pi[s_{1/2}^{-2}h_{9/2}i_{13/2}]_{11^-} \otimes \nu[i_{13/2}^{-1}]_{13/2^+}$ configuration at low rotational frequencies.

Despite these general similarities in the aligned-angular momentum behavior, the ^{189}Pb dipole band states do show some subtle differences to those of the heavier, odd-mass isotopes as plotted in Fig. 6(a). The main difference is that the initial aligned-angular momentum of the dipole band in ^{189}Pb is $\sim 2\hbar$ larger than that of the neighboring isotopes. The excitation energies of equivalent states in dipole bands from ^{191}Pb - ^{199}Pb are plotted versus mass number in Fig. 6(b). From this figure, it can be seen that states in the new dipole band in ^{189}Pb lie at a lower excitation energy than might be expected based on a systematic extrapolation from the higher-mass isotopes. Although the new results for ^{189}Pb appear to be the first nucleus to differ in trend from the heavier mass Pb isotopes, we note that the values for the band-head state of the dipole band in ^{191}Pb were published as tentative [2]. This is because, although internal conversion coefficients have been deduced for transitions below the band head in ^{191}Pb [27], it was difficult to rule out the fact that the decay path may pass through unobserved, low-energy transitions [2]. In view of this, the aligned-angular momenta and excitation energy

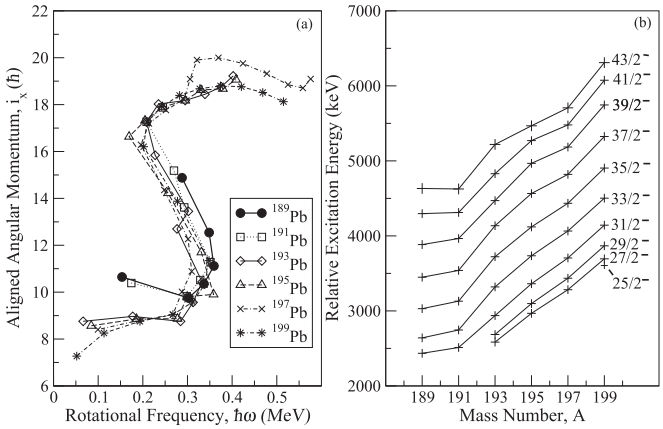

FIG. 7. Same as Fig. 6, but with the spins of the dipole band in ^{191}Pb raised by $1\hbar$ [3], see text for details.

systematics relative to the $13/2^+$ neutron-hole excitation shown in Fig. 6 have been replotted in Fig. 7 with the band-head spin of ^{191}Pb raised by $1\hbar$ [3].

In Fig. 7, with the ^{191}Pb data plotted with an increased band-head spin of $+1\hbar$, the aligned-angular momenta appear to follow a similar trend to that of the new dipole band in ^{189}Pb as a function of rotational frequency. A similar improved match is also seen in the excitation energy systematics versus mass number in Fig. 7(b). The increased aligned-angular momentum at low rotational frequencies in ^{189}Pb, and perhaps in ^{191}Pb, relative to the higher-mass isotopes may suggest that the lighter-mass dipole band-head states are subject to a smaller repulsive proton/neutron-hole interaction. This reduced repulsive interaction allows the angular momentum of the neutrons to contribute more to the total aligned-angular momentum at low rotational frequencies. At higher rotational frequencies, this becomes less noticeable as the proton and neutron-hole orbits align, see Fig. 6(a). A full theoretical study of the effects of the proton/neutron-hole interaction, including the new data for ^{189}Pb, would be very useful to interpret these systematic differences.

V. CONCLUSION

A new dipole band has been observed built upon the $I^\pi = 31/2^-$ isomeric state in ^{189}Pb based on a $\pi[s_{1/2}^{-2}h_{9/2}i_{13/2}]_{11^-} \otimes \nu[i_{13/2}^{-1}]_{13/2^+}$ configuration. The $M1$ multipolarities of the transitions in the band have been deduced from a combination of measured internal conversion coefficients and angular intensity ratios. The configuration that has been invoked for the most intense, negative parity, dipole bands in heavier odd-mass Pb nuclei is also invoked for the ^{189}Pb band due to systematic arguments. The aligned-angular momentum properties of the new ^{189}Pb band may suggest that subtle differences are occurring in the proton/neutron-hole interaction relative to dipole bands in the heavier mass Pb nuclei.

ACKNOWLEDGMENTS

This work has been supported by the EU 7th Framework Programme, "Integrating Activities Transnational Access", Project No. 262010 (ENSAR), and by the Academy of Finland under the Finnish Centre of Excellence Programme (Nuclear and Accelerator Based Physics Programme at JYFL). The authors acknowledge support of GAMMAPOOL for the JUROGAM detectors. D.H., D.M.C., M.G.P., and M.J.T. acknowledge support of the Science and Technology Facilities Council (STFC) through standard Grant EP/E02551X/1. T.G. acknowledges the support of the Academy of Finland Contract No. 131665. Useful discussions with G. Dracoulis, G. Lane, and T. Kibédi are gratefully acknowledged.

[1] K. Heyde and J. L. Wood, Rev. Mod. Phys. **83**, 1467 (2011).
[2] N. Fotiades *et al.*, Phys. Rev. C **57**, 1624 (1998).
[3] L. Ducroux *et al.*, Zeitschrift für Physik A Hadrons and Nuclei **356**, 241 (1996).
[4] M. Kaci *et al.*, Zeitschrift für Physik A Hadrons and Nuclei **354**, 267 (1996).
[5] A. Görgen *et al.*, Nucl. Phys. A **683**, 108 (2001).
[6] G. Baldsiefen *et al.*, Nucl. Phys. A **574**, 521 (1994).
[7] G. D. Dracoulis *et al.*, Phys. Rev. C **69**, 054318 (2004).
[8] G. Dracoulis, A. Byrne, and A. Baxter, Phys. Lett. B **432**, 37 (1998).
[9] J. R. Hughes *et al.*, Phys. Rev. C **51**, R447 (1995).
[10] G. D. Dracoulis, G. J. Lane, T. Kibédi, and P. Nieminen, Phys. Rev. C **79**, 031302 (2009).
[11] G. D. Dracoulis *et al.*, Phys. Rev. C **67**, 051301(R) (2003).
[12] H. Hübel, Prog. Part. Nucl. Phys. **54**, 1 (2005).
[13] R. M. Clark and A. O. Macchiavelli, Annu. Rev. Nucl. Part. Sci. **50**, 1 (2000).
[14] A. M. Baxter *et al.*, Phys. Rev. C **71**, 054302 (2005).
[15] P. Greenlees *et al.*, Eur. Phys. J. A **25**, 599 (2005).
[16] M. Leino *et al.*, Nucl. Instrum. Methods B **99**, 653 (1995).
[17] R. Page *et al.*, Nucl. Instrum. Methods B **204**, 634 (2003).
[18] I. Lazarus *et al.*, IEEE Trans. Nucl. Sci. **48**, 567 (2001).
[19] P. Rahkila, Nucl. Instrum. Methods A **595**, 637 (2008).
[20] D. Radford, Nucl. Instrum. Methods A **361**, 297 (1995).
[21] D. M. Cullen *et al.*, Phys. Rev. C **58**, 846 (1998).
[22] B. Singh, Nucl. Data Sheets **95**, 387 (2002).
[23] B. Singh, Nucl. Data Sheets **99**, 275 (2003).
[24] T. Kibédi, T. Burrows, M. Trzhaskovskaya, P. Davidson, and C. Nestor Jr., Nucl. Instrum. Methods A **589**, 202 (2008).
[25] M.-G. Porquet *et al.*, Phys. Rev. C **44**, 2445 (1991).
[26] D. L. Balabanski *et al.*, Phys. Rev. C **83**, 014304 (2011).
[27] J. Lagrange, M. Pautrat, J. Dionisio, C. Vieu, and J. Vanhorenbeeck, Nucl. Phys. A **648**, 64 (1999).